Modeling and Simulation of Propylene Polymerization in Nonideal Loop Reactors

A. S. Reginato, J. J. Zacca, and A. R. Secchi
Dept. of Chemical Engineering, UFRGS, Porto Alegre, RS, Brazil, CEP 90050-170

A dynamic mathematical model for liquid-phase polymerization in loop reactors was developed and implemented in language C using S-functions in a MATLAB/SIMULINK environment. It is based on a nonideal continuous stirred-tank reactor (CSTR) model capable of dealing with multisite copolymerization of olefins. The kinetic scheme includes a specific mechanism for hydrogen effect on the rate of polymerization observed on both laboratory experiments and industrial plant trials. A nonideality due to polymer segregation at the reactor output was inserted into the model to better predict reactor slurry density. Polymer moment balances were used to compute resin properties, such as average molecular weights, polydispersity, and melt flow index. Dynamic data from an industrial polypropylene plant were used for parameter estimation and model validation.

Introduction

Liquid-phase propylene polymerization is one of the most important industrial processes in polypropylene manufacture. This bulk process represents about 35% of total polypropylene production. Nevertheless, there have been relatively few publications about modeling loop reactors for olefin polymerization. Uvarov and Tsevetkova (1974), Lepski and Inkov (1977), and Ferrero and Chiovetta (1990) have modeled loop reactors as a CSTR. Zacca and Ray (1993) modeled loop reactors as two tubular sections interconnected by perfectly mixed inlet and outlet zones. A comprehensive kinetic scheme that was able to deal with multisite (up to four active site types) and copolymerization (up to three monomers, one of them a diene) kinetics was presented. However, no specific mechanism to deal with hydrogen effects on the polymerization rate was presented.

As shown by Zacca and Ray (1993), at high recycle ratios (= recycle volumetric flow rate/output volumetric flow rate), a loop reactor can be modeled as a CSTR. However, as explained by Ferrero and Chiovetta (1990), in practice, loop reactors can exhibit outlet polymer concentrations that differ from the ones inside the reactor. This happens because polymer particles may settle down in the reactor's leg due to centrifugal and gravitational forces, increasing the output concentration.

In the present work, mathematical modeling of loop reactors based upon a nonideal CSTR is developed for studying the macroscopic properties of the process, such as dynamics of the unit, advanced control strategies, grade transitions, and average polymer properties. The model is able to fit the observed outflow polymer concentrations of industrial reactors. A comprehensive kinetic scheme including important hydrogen effects on the rate of polymerization is presented. Kinetic and model parameters are estimated based on industrial plant data.

Correspondence concerning this article should be addressed to A. R. Secchi.

Process Description

The bulk process can produce polypropylene homopolymer suited for fiber applications with narrow molecular-weight distribution (MWD) and melt-flow index (MFI) ranging from 0.1 to 1,860 without the need of peroxide cracking (POPS, 2000). In soft material applications, the bulk process is able to achieve ethylene incorporation levels of up to 14%, corresponding to 25% rubber phase, in a single gas-phase reactor. In random copolymer production, it produces resins with up to 4.5 wt % of ethylene, and also terpolymer materials containing ethylene and butene.

Figure 1 shows the process: the catalyst (normally a fourth-generation Ziegler-Natta catalyst), previously activated by aluminum–alquil and treated with an external electron donor, is continuously fed into the first reactor along with the monomers and the chain transfer agent (hydrogen). The output from the first reactor, after mixing with a side feed stream containing monomers and chain transfer agent,

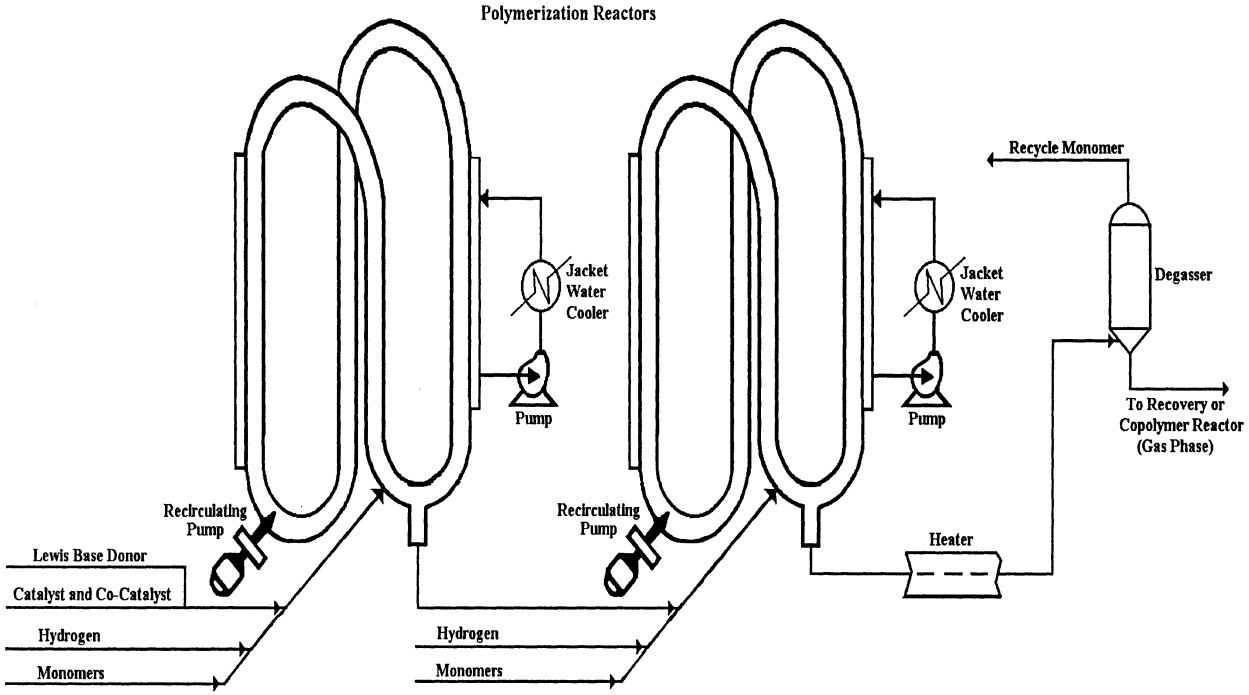

Figure 1. Bulk process.

is fed into the second loop reactor. The output stream from the second reactor is flashed to separate the solid phase (polymer) from the unreacted monomers. For homopolymer and random copolymers, the solid phase is deactivated with steam and then extruded. In the case of heterophasic (impact) copolymers, polymerization continues in a gas-phase reactor where the addition of the rubber phase [essentially ethylene–propylene rubber (EPR)] imparts better impact resistance (Galli and Ali, 1987). The loop reactor operates totally filled with slurry. An axial pump, placed in the lower part of the reactor, promotes a high-velocity (5–7 m/s) recycling of the reaction mixture. The resulting turbulent flow provides high heat transfer between the jacket coolant water and the reaction media.

Although the process can operate with a single loop reactor, normally it is designed with two loop reactors in series. One or two additional gas-phase reactors can be placed in series to produce heterophasic copolymers. The two-loop reactor system has the capability of producing bimodal resins with increased mechanical properties.

Process Modeling

Industrial loop reactors are typically operated under high recycle rates, in order to prevent polymer fouling (bulk velocity $\gg$ particle-free settling velocity) and to increase heat transfer. Under these conditions, it is possible to consider loop reactors as continuous stirred-tank reactors (CSTR) with constant volume, but variable reactor density. The reaction slurry is supposed to be a two-phase system composed of a liquid mixture (monomers, hydrogen, and solvent) and a solid-phase (polymer and catalyst). The following modeling assumptions are considered:

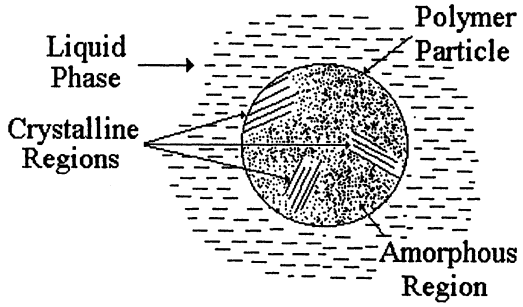

Figure 2. Semicrystalline polymer particle.

(1) The loop reactor does not present temperature and concentration gradients along its radial and axial coordinates (Zacca, 1991; Liang et al., 1996);

(2) Polymer particles are composed of two phases: crystalline and amorphous (Figure 2);

(3) The crystalline phase does not sorb any monomer (Hutchinson, 1990);

(4) Concentration in the amorphous phase can be related to liquid-phase concentration by an equilibrium partition constant (γ_j);

(5) Component equipartition is assumed. All partition constants ($\gamma_1 = \gamma_2 = \cdots = \gamma_{NC}$) are the same and the proportion of all diffusing species in the amorphous polymer phase equals the one in the liquid phase (Zacca, 1995);

(6) The effective concentration (concentration at the catalyst sites) is the same as in the amorphous polymer phase;

(7) The catalyst particles are monodisperse. The effects of the real calayst particle-size distribution (PSD), usually represented by a log-normal distribution, are lumped into a dis-

charge factor defined for the nonideal CSTR model. Moreover, the catalyst encapsulation, used in industrial processes and carried out in a prepolymerization reactor upstream from the loop reactors, decrease fines generation in the system, giving a PSD closer to the monodisperse case (Zacca and Debling, 2001). In order to capture more rigorously the distributed nature of the problem, population balances on the growing particles are necessary (see, for example, Kim and Choi, 2001; Mattos Neto and Pinto, 2001; Zacca and Debling, 2001) together with fluid-dynamic modeling to take into account the centrifugal and gravitational forces. However, for the purpose of the proposed model, these additional complexities were not considered.

Olefin polymerization kinetics with Ziegler-Natta catalysts can be quite complex. Several reaction steps have been postulated in the specialized literature (Zacca, 1991, 1995; Soares and Hamielec, 1996 a,b; Carvalho et al., 1989; Samson et al., 1999; and Rishina et al., 1993). The basic kinetic model used in this work is summarized in Table 1. Some new reaction steps have been added to the model with specific objectives. A dead site reactivation by hydrogen was included as a possible way to account for the hydrogen activation effect on polymerization rate. Donor deactivation by poison was also included in order to explain the observed increase in the fraction of soluble polymer in the presence of raw material impurities.

From the reaction steps in Table 1, the following rate equations can be written

Hydrogen

$$R_H = -\sum_{k=1}^{Ns}\left[R_{aH}^k + R_{rH}^k + R_{dH0}^k + \sum_{i=1}^{Nm}\sum_{\boldsymbol{n}=\boldsymbol{\delta}_i}^{\infty}\left(R_{cHi}^{k,\boldsymbol{n}} + R_{dHi}^{k,\boldsymbol{n}}\right)\right] \tag{1}$$

Electron donor

$$R_E = -\sum_{k=1}^{Ns}\left[R_{dE0}^k + \sum_{\substack{l=1\\ l\neq k}}^{Ns} R_{tE0}^{kl} + \sum_{i=1}^{Nm}\sum_{\boldsymbol{n}=\boldsymbol{\delta}_i}^{\infty}\left(\sum_{\substack{l=1\\ l\neq k}}^{Ns} R_{tEi}^{lk,\boldsymbol{n}} + R_{dEi}^{k,\boldsymbol{n}}\right)\right] - R_{eE} \tag{2}$$

Cocatalyst

$$R_A = -\sum_{k=1}^{Ns}\left[R_{aA}^k + R_{dA0}^k + \sum_{i=1}^{Nm}\sum_{\boldsymbol{n}=\boldsymbol{\delta}_i}^{\infty} R_{dAi}^{k,\boldsymbol{n}}\right] - R_{eA} \tag{3}$$

Table 1. Kinetic Model

Reaction Step	Component	Reaction	Rate Equation
Site activation	Hydrogen	$C_P + H_2 \rightarrow P_0^k$	$R_{aH}^k = k_{aH}^k C_P C_{H,a}^{O_{aH}^k}$
	Al-alkyl	$C_P + A \rightarrow P_0^k + B$	$R_{aA}^k = k_{aA}^k C_P C_{A,a}^{O_{aA}^k}$
	Monomer i	$C_P + M_i \rightarrow P_0^k + M_i$	$R_{aM_i}^k = k_{aM_i}^k C_P C_{M_i}^{O_{aM_i}^k}$
	Spontaneous	$C_P \rightarrow P_0^k$	$R_{aSp}^k = k_{aSp}^k C_P$
Chain initiation	Monomer i	$P_0^k + M_i \rightarrow P_{\boldsymbol{\delta}_i,i}^k$	$R_{P0i}^k = k_{P0i}^k P_0^k C_{M_i,a}$
Chain propagation	Monomer j	$P_{\boldsymbol{n},i}^k + M_j \rightarrow P_{\boldsymbol{n}+\boldsymbol{\delta}_j,j}^k$	$R_{Pji}^{k,\boldsymbol{n}} = k_{Pji}^k P_{\boldsymbol{n},j}^k C_{M_j,a}$
Chain transfer	Hydrogen	$P_{\boldsymbol{n},i}^k + H_2 \rightarrow P_0^k + D_{\boldsymbol{n}}^k$	$R_{cHi}^{k,\boldsymbol{n}} = k_{cHi}^k P_{\boldsymbol{n},i}^k C_{H,a}^{O_{cHi}^k}$
	Monomer j	$P_{\boldsymbol{n},i}^k + M_j \rightarrow P_{\delta_j,j}^k + D_{\boldsymbol{n}}^k$	$R_{cM_{ji}}^{k,\boldsymbol{n}} = k_{cM_{j,i}}^k P_{\boldsymbol{n},i}^k C_{M_j,a}^{O_{cM_j,i}^k}$
	Spontaneous	$P_{\boldsymbol{n},i}^k \rightarrow D_{\boldsymbol{n}}^k + P_0^k$	$R_{cSpi}^{k,\boldsymbol{n}} = k_{cSpi}^k P_{\boldsymbol{n},i}^k$
Site deactivation	Hydrogen	$P_{\boldsymbol{n},i}^k + H_2 \rightarrow C_d + D_{\boldsymbol{n}}^k$	$R_{dHi}^{k,\boldsymbol{n}} = k_{dH}^k P_{\boldsymbol{n},i}^k C_{H,a}^{O_{dH}^k}$
		$P_0^k + H_2 \rightarrow C_d$	$R_{dH0}^k = k_{dH}^k P_0^k C_{H,a}^{O_{dH}^k}$
	Electron donor	$P_{\boldsymbol{n},i}^k + E \rightarrow C_d + D_{\boldsymbol{n}}^k$	$R_{dEi}^{k,\boldsymbol{n}} = k_{dE}^k P_{\boldsymbol{n},i}^k C_{E,a}^{O_{dE}^k}$
		$P_0^k + E \rightarrow C_d$	$R_{dE0}^k = k_{dE}^k P_0^k C_{E,a}^{O_{dE}^k}$
	Al-alkyl	$P_{\boldsymbol{n},i}^k + A \rightarrow C_d + D_{\boldsymbol{n}}^k$	$R_{dAi}^{k,\boldsymbol{n}} = k_{dA}^k P_{\boldsymbol{n},i}^k C_{A,a}^{O_{dA}^k}$
		$P_0^k + A \rightarrow C_d$	$R_{dA0}^k = k_{dA}^k P_0^k C_{A,a}^{O_{dA}^k}$
	Poison	$P_{\boldsymbol{n},i}^k + X \rightarrow C_d + D_{\boldsymbol{n}}^k$	$R_{dXi}^{k,\boldsymbol{n}} = k_{dX}^k P_{\boldsymbol{n},i}^k C_{X,a}^{O_{dX}^k}$
		$P_0^k + X \rightarrow C_d$	$R_{dX0}^k = k_{dX}^k P_0^k C_{X,a}^{O_{dX}^k}$
	Spontaneous	$P_{\boldsymbol{n},i}^k \rightarrow C_d + D_{\boldsymbol{n}}^k$	$R_{dSpi}^{k,\boldsymbol{n}} = k_{dSp}^k P_{\boldsymbol{n},i}^k$
		$P_0^k \rightarrow C_d$	$R_{dSp0}^k = k_{dSp}^k P_0^k$
Site transformation	Donor	$P_{\boldsymbol{n},i}^k + E \rightarrow P_0^l + D_{\boldsymbol{n}}^k$	$R_{tEi}^{kl,\boldsymbol{n}} = k_{tE}^{kl} P_{\boldsymbol{n},i}^k C_{E,a}^{O_{tE}^{kl}}$
		$P_0^k + E \rightarrow P_0^l$	$R_{tE0}^{kl} = k_{tE}^{kl} P_0^k C_{E,a}^{O_{tE}^{kl}}$
	Spontaneous	$P_{\boldsymbol{n},i}^k \rightarrow P_0^l + D_{\boldsymbol{n}}^k$	$R_{tSpi}^{kl,\boldsymbol{n}} = k_{tSp}^{kl} P_{\boldsymbol{n},i}^k$
		$P_0^k \rightarrow P_0^l$	$R_{tSp0}^{kl} = k_{tSp}^{kl} P_0^k$
Dead site reactivation	Hydrogen	$C_d + H_2 \rightarrow P_0^k$	$R_{rH}^k = k_{rH}^k C_d C_{H,a}^{O_{rH}^k}$
Poison deactivation	Al-alkyl	$A + X \rightarrow B$	$R_{eA} = k_{eA} C_{A,a}^{O_{eX}} C_{X,a}^{O_{eX}}$
Donor deactivation	Poison	$E + X \rightarrow B$	$R_{eE} = k_{eE} C_{E,a}^{O_{eE}} C_{X,a}$

Poison

$$R_X = -\sum_{k=1}^{Ns}\left[R^k_{dX0} + \sum_{i=1}^{Nm}\sum_{\boldsymbol{n}=\boldsymbol{\delta}_i}^{\infty} R^{k,\boldsymbol{n}}_{dXi}\right] - R_{eE} - R_{eA} \quad (4)$$

Potential sites

$$R_{Cp} = -\sum_{k=1}^{Ns}\left(R^k_{aH} + R^k_{aA} + R^k_{aSp} + \sum_{i=1}^{Nm} R^k_{aM_i}\right) \quad (5)$$

Vacant sites

$$\begin{aligned} R_{P^k_0} = {} & R^k_{aH} + R^k_{aA} + R^k_{aSp} + \sum_{i=1}^{Nm} R^k_{aM_i} + R^k_{rH} - R^k_{dH0} - R^k_{dE0} \\ & - R^k_{dA0} - R^k_{dSp0} - R^k_{dX0} - \sum_{j=1}^{Nm} R^k_{P0j} \\ & + \sum_{i=1}^{Nm}\sum_{\boldsymbol{n}=\boldsymbol{\delta}_i}^{\infty}\left(R^{k,\boldsymbol{n}}_{cHi} + R^{k,\boldsymbol{n}}_{cSpi}\right) \\ & + \sum_{i=1}^{Nm}\sum_{\substack{l=1\\ l\neq k}}^{N_S}\sum_{\boldsymbol{n}=\boldsymbol{\delta}_i}^{\infty}\left(R^{lk,\boldsymbol{n}}_{tEi} + R^{lk,\boldsymbol{n}}_{tSpi}\right) \\ & + \sum_{\substack{l=1\\ l\neq k}}^{N_S}\left(R^{lk}_{tE0} + R^{lk}_{tSp0} - R^{kl}_{tE0} - R^{kl}_{tSp0}\right) \end{aligned} \quad (6)$$

Dead sites

$$R_{Cd} = \sum_{k=1}^{Ns}\left[\begin{array}{l}\left(R^k_{dH0} + R^k_{dE0} + R^k_{dA0} + R^k_{dX0} + R^k_{dSp0} - R^k_{rH}\right) + \\ \sum_{i=1}^{Nm}\sum_{\boldsymbol{n}=\boldsymbol{\delta}_i}^{\infty}\left(R^{k,\boldsymbol{n}}_{dHi} + R^{k,\boldsymbol{n}}_{dEi} + R^{k,\boldsymbol{n}}_{dAi} + R^{k,\boldsymbol{n}}_{dXi} + R^{k,\boldsymbol{n}}_{dSpi}\right)\end{array}\right] \quad (7)$$

Monomer

$$R_{M_i} = -\sum_{k=1}^{Ns}\left[R^k_{P0i} + \sum_{j=1}^{Nm}\sum_{\boldsymbol{n}=\boldsymbol{\delta}_i}^{\infty}\left(R^{k,\boldsymbol{n}}_{Pij} + R^{k,\boldsymbol{n}}_{cM_i,j}\right)\right] \quad (8)$$

Live polymer

$$\begin{aligned} R_{P^k_{\boldsymbol{n},i}} = {} & \delta(\boldsymbol{n}-\boldsymbol{\delta}_i)\left[R^k_{P0i} + \sum_{j=1}^{Nm}\sum_{\boldsymbol{m}=\boldsymbol{\delta}_j}^{\infty} R^{k,\boldsymbol{m}}_{cM_i,j}\right] \\ & + \sum_{j=1}^{Nm} k^k_{P_{ij}} C_{M_i,a} P^k_{\boldsymbol{n}-\boldsymbol{\delta}_i,j} - \sum_{j=1}^{Nm} k^k_{P_{ji}} C_{M_j,a} P^k_{\boldsymbol{n},i} - \alpha^k_i P^k_{\boldsymbol{n},i} \end{aligned} \quad (9)$$

Dead polymer

$$R_{D^k_{\boldsymbol{n}}} = \sum_{i=1}^{Nm} \alpha^k_i P^i_{\boldsymbol{n},i} \quad (10)$$

where

$$\begin{aligned} \alpha^k_i = {} & k^k_{cHi} C^{O^k_{cHi}}_{H,a} + k^k_{cSpi} + \sum_{j=1}^{Nm} k^k_{cM_j,i} C_{M_j,a} \\ & + \sum_{\substack{l=1\\ l\neq k}}^{N_S}\left(k^{kl}_{tEi} C^{O^{kl}_{tE}}_{E,a} + k^{kl}_{tSpi}\right) \\ & + k^k_{dHi} C^{O^k_{dH}}_{H,a} + k^k_{dAi} C^{O^k_{dA}}_{A,a} + k^k_{dEi} C^{O^k_{dE}}_{E,a} \\ & + k^k_{dXi} C^{O^k_{dX}}_{X,a} + k^k_{dSpi} \end{aligned} \quad (11)$$

Polymer moment rate equations

In this model, multisite copolymer moments are defined as

$$\mu^k_{\boldsymbol{\delta}_l,i} = \sum_{\boldsymbol{n}=\mathbf{1}}^{\infty} \boldsymbol{n}^{\boldsymbol{\delta}_l} P^k_{\boldsymbol{n},i} \quad (12)$$

$$\lambda^k_{\boldsymbol{\delta}_l} = \sum_{\boldsymbol{n}=\boldsymbol{\delta}_i}^{\infty}\left(\sum_{i=1}^{Nm} P^k_{\boldsymbol{n},i} + D^k_{\boldsymbol{n}}\right) \quad (13)$$

for live and bulk polymers, respectively. Then, the moment rate equations become as follows

Zero-order live polymer moments

$$\begin{aligned} R_{\mu^k_{\mathbf{0},i}} = {} & R^k_{P0i} + \sum_{j=1}^{Nm} k^k_{cM_i,j} C_{M_i,a}\,\mu^k_{\mathbf{0},j} - \alpha^k_i \mu^k_{\mathbf{0},i} \\ & + \sum_{j=1}^{Nm}\left[k^k_{P_{ij}} C_{M_i,a}\,\mu^k_{\mathbf{0},j} - k^k_{P_{ji}} C_{M_j,a}\,\mu^k_{\mathbf{0},i}\right] \end{aligned} \quad (14)$$

Zero-order bulk polymer moments

$$R_{\lambda^k_{\mathbf{0}}} = \sum_{i=1}^{Nm}\left[R^k_{P0i} + \sum_{j=1}^{Nm} k^k_{cM_i,j} C_{M_i,a}\,\mu^k_{\mathbf{0},j}\right] \quad (15)$$

First-order live polymer moments

$$\begin{aligned} R_{\mu^k_{\boldsymbol{\delta}_l}} = {} & \sum_{i=1}^{Nm}\delta(i-l)\left[R^k_{P0i} + \sum_{j=1}^{Nm} k^k_{cM_i,j} C_{M_i,a}\,\mu^k_{\mathbf{0},j}\right] \\ & - \sum_{i=1}^{Nm}\alpha^k_i \mu^k_{\boldsymbol{\delta}_l,i} + \sum_{i=1}^{Nm}\sum_{j=1}^{Nm} k^k_{P_{ij}} C_{M_i,a}\,\delta(i-l)\,\mu^k_{\mathbf{0},j} \end{aligned} \quad (16)$$

First-order bulk polymer moments

$$\begin{aligned} R_{\lambda^k_{\boldsymbol{\delta}_l}} = {} & \sum_{i=1}^{Nm}\delta(i-l)\left[R^k_{P0i} + \sum_{j=1}^{Nm} k^k_{cM_i,j} C_{M_i,a}\,\mu^k_{\mathbf{0},j}\right] \\ & + \sum_{i=1}^{Nm}\sum_{j=1}^{Nm}\delta(i-l) k^k_{P_{ij}} C_{M_i,a}\,\mu^k_{\mathbf{0},j} \end{aligned} \quad (17)$$

Second-order bulk polymer moments

$$R_{\lambda_2} = \sum_{k=1}^{Ns} \sum_{j=1}^{Nm} \left[R_{P0j}^k + \sum_{i=1}^{Nm} k_{cM_j,i}^k C_{M_j,a} \mu_{\mathbf{0},i}^k \right] + \sum_{k=1}^{Ns} \sum_{i=1}^{Nm} \sum_{j=1}^{Nm} k_{Pji}^k C_{M_j,a} \left(\mu_{\mathbf{0},i}^k + 2\mu_{\mathbf{1},i}^k \right) \quad (18)$$

Equations 1–10 and 14–18 represent the kinetic-rate equations. Notice that most of these rates depend on the effective concentrations of amorphous polymer-phase components. For the sake of simplicity, it is more convenient to express the overall component balance in terms of bulk (total) concentrations ($C_{j,R}$)

$$C_{j,R} = \frac{\text{Moles of } j}{\text{Total volume}} \quad \text{for} \quad j = 1, 2, \ldots, NC \quad (19)$$

It is then necessary to find a way to relate effective (amorphous phase) and bulk (total) concentrations. The effective concentration of each component is related to its liquid-phase concentration by an equilibrium constant (γ) (Hutchinson, 1990)

$$\gamma_j = \frac{C_{j,a}}{C_{j,l}} \quad \text{for} \quad j = 1, 2, \ldots, NC \quad (20)$$

where $C_{j,a}$ is the effective amorphous-phase concentration and $C_{j,l}$ is the liquid-phase concentration. For a semicrystalline polymer particle, the swelling factor (χ) is defined as

$$\chi = \frac{V_{l,a}}{V_{a,m}} \quad (21)$$

where $V_{l,a}$ is the volume of liquid sorbed in the amorphous-polymer phase and $V_{a,m}$ is the volume of swelled amorphous phase.

Considering the crystallinity (f_c) as the fraction between crystalline and total polymer volume, $f_c = (V_c/V_{P,s})$, and the volumetric polymer fraction as $\phi_P = (V_{P,s}/V_R)$, where V_R is the reactor volume, it can be shown (Appendix A) that

$$\frac{C_{j,a}}{C_{j,R}} = \left(\frac{V_l}{V_{a,m}} + \frac{1-\chi}{1-f_c} + \chi \right) \frac{\gamma_j \dfrac{V_{a,m}}{V_l}}{1 + \gamma_j \dfrac{V_{a,m}}{V_l}} \quad (22)$$

where

$$\frac{V_l}{V_{a,m}} = \frac{1-\chi}{1-f_c} \left(\frac{1}{\phi_P} - 1 \right) - \chi \quad (23)$$

V_l is the liquid-phase volume, and $C_{j,R}$ is the bulk concentration. Equation 22 is used to relate the effective concentration ($C_{j,a}$) to the bulk concentration ($C_{j,R}$) in the balance equations.

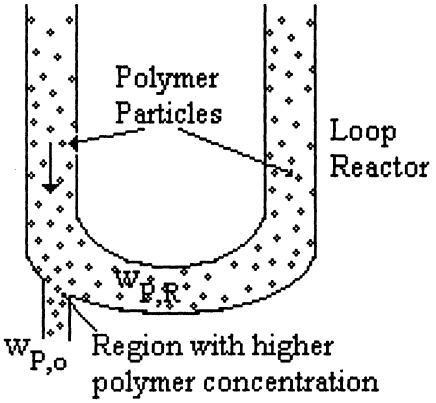

Figure 3. Nonideal CSTR.

Nonideal CSTR model

It is known that loop reactors operating under typical industrial conditions may be modeled as CSTRs (Zacca and Ray, 1993). In practice, however, loop reactors tend to show nonideal mixing behavior as a result of particle segregation. The concentration of solid particles in the reactor may change as a result of centrifugal forces (due to high-speed circulation) or the utilization of size-selection equipment. Settling legs and hydrocyclones are often used in order to improve downstream equipment efficiency due to decreased liquid inventories. The net result is that the outflow solids concentration is usually different than the average solids concentration inside the reactor. Polymer particles have a residence-time distribution that is different from the liquid phase. This important fact must be properly modeled, since it affects the overall mass balance in the system. It leads to a nonideal CSTR view of the system, as shown in Figure 3. To quantify the difference between the polymer concentration inside the reactor and the one at the reactor output, a discharge factor, D_f, is defined as the ratio between the output polymer weight fraction, $w_{P,o}$, and the reactor polymer weight fraction, $w_{P,R}$

$$D_f = \frac{w_{P,o}}{w_{P,R}} \quad (24)$$

The nonideal CSTR is equivalent to the flow sheet shown in Figure 4. A separation node (splitter) that recycles a certain amount of liquid/solid adjusts for the observed outlet solids concentration. The recycled stream is composed of only the liquid phase when $D_f > 1$, and only the solid phase when $D_f < 1$ (less polymer in the output stream than inside the reactor). When $D_f = 1$, no recycle is needed (ideal CSTR).

The discharge factor has a strong influence on reactor behavior. It affects reactor concentrations and slurry density. The ratio (η) between the liquid-phase concentration inside the reactor and at the output stream can be computed as (Appendix B)

$$\eta = \frac{C_{j,o}}{C_{j,R}} = \frac{\rho_o}{\rho_R} \frac{1 - D_f \cdot w_{P,R}}{1 - w_{P,R}} \quad (25)$$

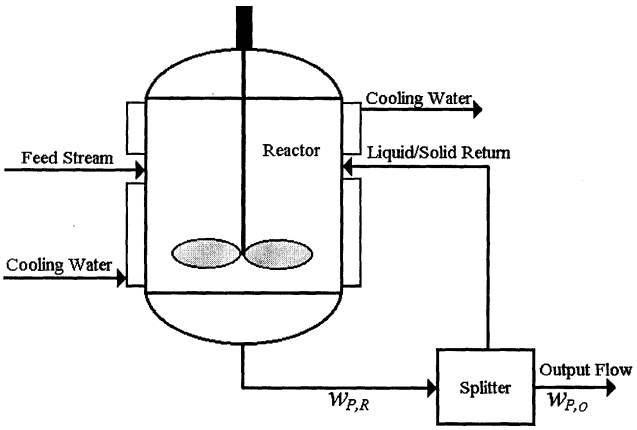

Figure 4. Nonideal CSTR flow-sheet representation.

where the densities at the reactor output ρ_o and inside the reactor ρ_R are obtained, respectively, by

$$\frac{1}{\rho_o} = \frac{1 - D_f \cdot w_{P,R}}{\rho_l} + \frac{D_f \cdot w_{P,R}}{\rho_P} \tag{26}$$

$$\frac{1}{\rho_R} = \frac{1 - w_{P,R}}{\rho_l} + \frac{w_{P,R}}{\rho_P} \tag{27}$$

where the liquid-phase density, ρ_l, is calculated by volume additivity of monomers and solvent densities.

Similar to the liquid phase, the solid phase (catalyst, live, and bulk polymer moments) concentration at the output can be computed from the following relation (Appendix B)

$$\xi = \frac{C_{j,o}}{C_{j,R}} = \frac{\rho_o}{\rho_R} D_f \tag{28}$$

In this way, a generic component balance is given by

$$\frac{dC_{j,R}}{dt} = \frac{Q_f C_{j,f}}{V_R} - \frac{(\eta|\xi) Q_o C_{j,R}}{V_R} + R_j \tag{29}$$

where

$$(\eta|\xi) = \begin{cases} \eta & \text{for liquid-phase components} \\ \xi & \text{for solid-phase components} \end{cases}$$

Since loop reactors operate at all times totally filled with reaction slurry, the total volume is considered to be constant, although density is allowed to vary according to monomer conversion to polymer. Therefore, a total mass balance in the reactor yields

$$V_R \frac{d\rho_R}{dt} = Q_f \rho_f - Q_o \rho_o \tag{30}$$

By writing the density as the volumetric sum of the component densities

$$\rho_R = \sum_{i=1}^{NC} \phi_i \rho_i + \phi_{P,R} \rho_P \tag{31}$$

and substituting its time derivative into Eq. 30, the output volumetric flow rate is given by

$$Q_o = Q_f \frac{\dfrac{\rho_f}{\rho_o} - \displaystyle\sum_{j=1}^{NC} \frac{\rho_j - \rho_P}{\rho_j} \frac{\overline{M}_j}{\rho_o} \left(C_{j,f} + \frac{V_R R_j}{Q_f} \right)}{1 - \eta \displaystyle\sum_{j=1}^{NC} \frac{\rho_j - \rho_P}{\rho_j} \frac{\overline{M}_j}{\rho_o} C_j} \tag{32}$$

where Q_o is seen to depend mainly on reaction rates, and reactor nonideality is represented by the η factor.

Under the usual considerations of no heat of mixing, no viscous heating, no external field effects, no radiation, and no expansion heat, the energy balance for the loop reactors can be written as (Froment and Bischoff, 1979)

$$\frac{dT}{dt} = \frac{1}{\rho V_R C_{pm}} \left(\rho_f Q_f \sum_{j=1}^{NC} w_j \int_T^{T_f} C_{p_j} \, dT + V_R \sum_{j=1}^{Nm} \left(-\Delta H_j R_j \right) + U A_t (T_w - T) \right) \tag{33}$$

where U is the global heat-transfer coefficient, A_t is the heat-exchange area, ΔH is the polymerization heat, C_{pm} is the mixture specific heat, and w_j is the weight fraction of component j.

Loop reactors have cooling jackets to promote heat removal from reaction media. A heat balance in the jacket, considering constant coolant-specific heat and density, is shown in the following equation

$$\frac{dT_w}{dt} = \frac{Q_w}{V_w} (T_{wf} - T_w) + \frac{U A_t}{\rho_w C_{Pw} V_w} (T - T_w) \tag{34}$$

where the subscript w refers to coolant water; Q_w, T_w, and T_{wf} represent the volumetric flow, jacket temperature, and feed temperature of cooling water, respectively; and V_w represents the jacket volume.

Polymer properties

Using polymer moments, it is possible to calculate the average polymer properties (Zacca, 1991; Zacca, 1995; Hutchinson, 1990; Chen, 1991). From basic polymer properties, such as average molecular weights (Eqs. 35 and 36), it is also possible to estimate end-use properties by means of empirical correlation

$$\overline{M}_n = \sum_{k=1}^{Ns} \sum_{i=1}^{Nm} \frac{\lambda_{\delta_i}^k}{\lambda_{\mathbf{0}}^k} \overline{M}_i \tag{35}$$

$$\overline{M}_w = \lambda_2 \cdot \sum_{k=1}^{Ns} \lambda_{\mathbf{0}}^k \overline{M}_n \Big/ \left(\sum_{k=1}^{Ns} \sum_{i=1}^{Nm} \lambda_{\delta_i}^k \right)^2 \tag{36}$$

Polypropylene melt flow index is normally related to mass-average molecular weight through a power-law-type correla-

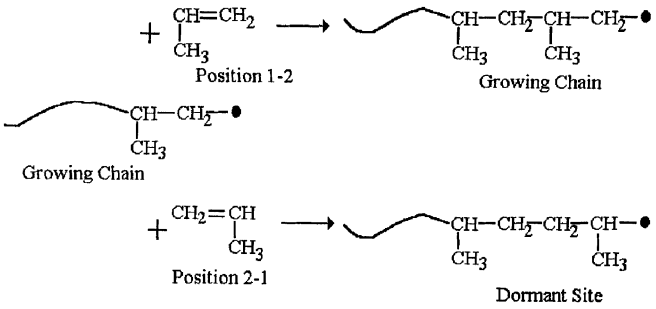

Figure 5. Dormant site generation.

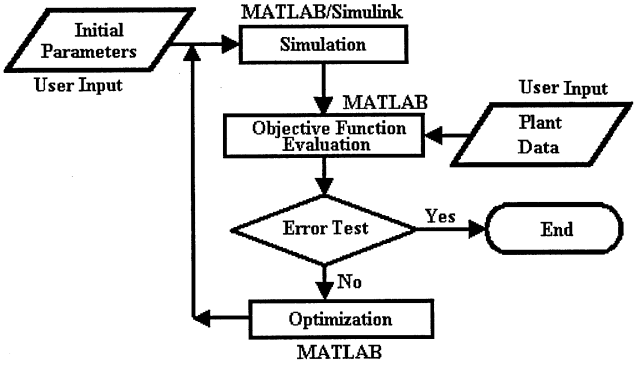

Figure 6. Parameter estimation method.

tion (Eq. 37)

$$MFI = a \cdot \left(\overline{M}_w\right)^b \tag{37}$$

with $a = 3.39 \cdot 10^{22}$ and $b = -3.92$ (Bremner and Rudin, 1990).

Hydrogen Effect on Polymerization

Hydrogen acts mainly in two different ways in liquid-phase propylene polymerization. It is a chain transfer agent that regulates the average molecular weight. As a secondary effect, hydrogen increases the polymerization rate. In the literature, different interpretations can be found for this effect. Parson and Al-Turki (1989), Rishina et al. (1994), and Soares and Hamielec (1996a) proposed an increase in the number of active sites when hydrogen is present in the reaction media. Samson et al. (1999) and Mori et al. (1998) suggested that dormant site reactivation by hydrogen is the polymerization rate-enhancement mechanism. A dormant site (Corradini et al., 1992) is an active site after a 2–1 propylene insertion that generates a secondary Ti–C bond (Figure 5). The steric hindrance of a methyl group closer to the catalyst site slows down polymerization until a chain transfer reaction occurs.

In order to allow the creation of new active sites in the kinetic scheme, two additional reactions were proposed: potential-site activation and dead-site reactivation by hydrogen. The dormant-site reactivation mechanism was included as an equilibrium reaction between two types of sites.

In practice, plant data show that hydrogen rate enhancement may be as high as doubling the polymerization rate. To take this effect into account, a pseudo two-site model was considered (Table 1). Hydrogen is considered to transform sites of type 1 into sites of type 2 through an equilibrium mechanism, as shown in Eq. 38 (Reginato, 2001)

$$C^1 + H_2 \underset{k_{-a}}{\overset{k_a}{\leftrightarrow}} C^2 \tag{38}$$

According to this model, if k_P^1 and k_P^2 are the propagation rate constants of sites 1 (C^1) and 2 (C^2), respectively, it can be shown (Appendix C) that the effective propagation rate constant ($k_{P,r}$) is given by

$$k_{P,r} = k_P^1 \frac{1 + K\dfrac{k_P^2}{k_P^1} C_{H,a}}{1 + KC_{H,a}} \tag{39}$$

where $K = k_a/k_{-a}$ is the two-site interconversion equilibrium constant.

Results

The dynamic mathematical model consists of a set of nonlinear ordinary differential equations relative to the balances of solvent, hydrogen, electron-donor, cocatalyst, poison, potential, dead and vacant sites, monomers, slurry density, and polymer moments. This model was implemented as a MATLAB S-function in C language and solved with a backward differentiation formula (BDF) algorithm (Shampine and Reichelt, 1998).

Parameter estimation was performed for a single-site model in the case of propylene homopolymerization, using industrial data (see Figure 10). The parameter estimation procedure is illustrated in Figure 6, where the Nelder-Mead (Secchi and Bolsoni, 1998) optimization algorithm was used to minimize the following objective function

$$S(\hat{\alpha}) = \frac{1}{M}\sum_{j=1}^{M}\left(\frac{w_j^e}{N}\sum_{i=1}^{N} w_i\left(\frac{y_{ij}^{\exp} - y_{ij}}{y_{ij}^{\exp}}\right)^2\right) \tag{40}$$

where M is the number of output variables, N is the number of data points, w_i is the weighting factor for each data point, w_j^e is the weighting factor for each output variable, and y_{ij} is the data point i corresponding to output j.

The implemented model is quite complex and aims to deal with a wide range of phenomena in liquid-phase propylene polymerization. For the purpose of this work, a simplified model was derived from it so it would be possible to estimate parameters with industrial data only. Some reaction components, like poison, Al-alkyl, and electron donor has no measure or has no significant variation to estimate parameters related to their reactions. The site-activation reactions are carried out in a prepolymerization reactor that was not mod-

Table 2. Parameter Sensitivity Analysis

Outputs	Parameters										
	k_{aH}	k_{P0}	k_P	k_{cH}	k_{dH}	k_{dsp}	k_{rH}	$K\frac{k_P^2}{k_P^1}$	K	D_{f1}	D_{f2}
ρ_{R1}	0.014	0.0012	0.44	−0.018	−0.010	−0.128	0.024	0.14	−0.09	−0.71	0
$\overline{M}w_1$	−0.009	−0.0008	0.67	−0.950	0.007	0.083	−0.016	0.21	−0.14	0.27	0
P_1	0.051	0.0043	1.52	−0.062	−0.035	−0.444	0.084	0.48	−0.31	−1.45	0
ρ_{R2}	0.018	0.0013	0.46	−0.020	−0.013	−0.157	0.034	0.15	−0.09	−0.29	−0.44
$\overline{M}w_2$	−0.010	−0.0008	0.66	−0.950	0.007	0.091	−0.018	0.21	−0.14	0.24	0.04
P_2	0.079	0.004	1.60	−0.079	−0.053	−0.663	0.169	0.52	−0.33	−0.08	−1.29

Table 3. Input Sensitivity Analysis

Outputs	Inputs				
	$\dot{m}_{C3,f1}$	$C_{H,f1}$	$\dot{m}_{CAT,f}$	$\dot{m}_{C3,f2}$	$C_{H,f2}$
ρ_{R1}	−0.751	0.139	0.425	0	0
$\overline{M}w_1$	0.490	−0.386	−0.278	0	0
P_1	−1.600	0.480	1.472	0	0
ρ_{R2}	−0.631	0.143	0.450	−0.152	0.015
$\overline{M}w_2$	0.464	−0.351	−0.286	0.037	−0.039
P_2	−1.105	0.462	1.525	−0.478	0.141

Table 4. Main Parameters and Operating Conditions

Parameters	Value	Units
k_P	463*	$m^3 kgmol^{-1} s^{-1}$
k_{cH}	22.7*	$(m^3)^{0.5}(kgmol)^{-0.5} s^{-1}$
k_{dsp}	3.2×10^{-4}*	s^{-1}
$\frac{k_P^2}{k_P^1}$	1.8	—
K	125	$kgmol^{-1}$
D_{f1}	1.25	—
D_{f2}	1.10	—
A_t	20	m^2
ΔH	-8.8×10^4	kJ $kgmol^{-1}$
U	41.7	kJ m^{-2} K^{-1} s^{-1}
V_R	45	m^3
V_w	10	m^3

*Values at 70°C.

eled in this work. Only site activation by hydrogen was considered in a first moment to try to explain the hydrogen effect on polymer production rate. Chain transfer to monomer and spontaneous chain transfer are less significant when compared to transfer to hydrogen. Site-transformation reactions are intended to explain the isotactic index of the polymer that is not considered in this work. These reaction steps will be considered in future works.

After these previous selections, the reaction steps considered in this work are: site activation by hydrogen, chain initiation, chain propagation, chain transfer to hydrogen, site deactivation by hydrogen and spontaneous, dead-site reactivation by hydrogen, and the two-site equilibrium presented before.

Based on this simplified model, a parametric sensitivity analysis was carried out to determine which parameters are more important in adjusting the mathematical model to actual data. Input sensitivity analysis was also accomplished to find out which inputs can be used to estimate related parameters. Tables 2 and 3 shows the sensitivity analysis results. From Table 2 it can be stated that site activation by hydrogen, chain initiation, site deactivation by hydrogen, and site reactivation by hydrogen are not very important. From Table 3 it can be stated that all inputs have a significant influence on outputs.

From the previous discussion, it can be considered that the catalyst is totally activated when it is fed into the reactor system and the following reaction steps are included: chain propagation, chain transfer to hydrogen, spontaneous site deactivation, and the two site interconversion equilibrium (hydrogen effect). Discharge factors were also included. The estimated parameters are presented later in Table 4.

Discharge factor influence

Figure 7 shows the effect of D_f on slurry density and concentrations, under constant process inputs and reactor production. For these conditions, the outlet slurry density (ρ_o) is constant. In the case of an ideal CSTR ($D_f = 1$), concentrations and slurry density inside the reactor (ρ_R) are equal to their counterparts in the output stream.

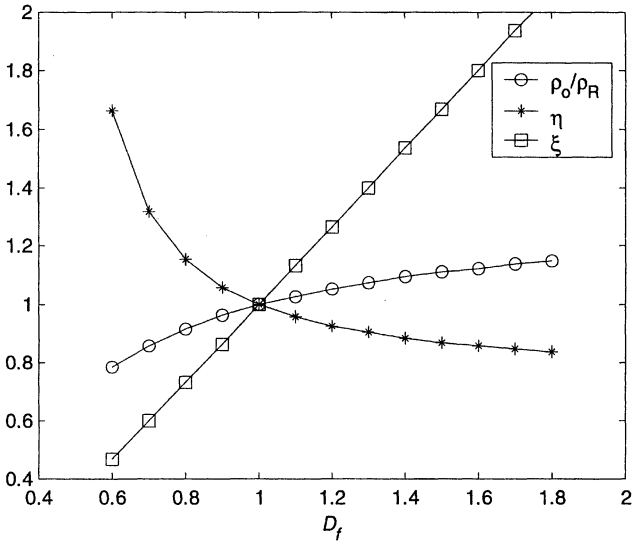

Figure 7. Influence of D_f on reactor slurry density and concentration for constant production and process inputs.

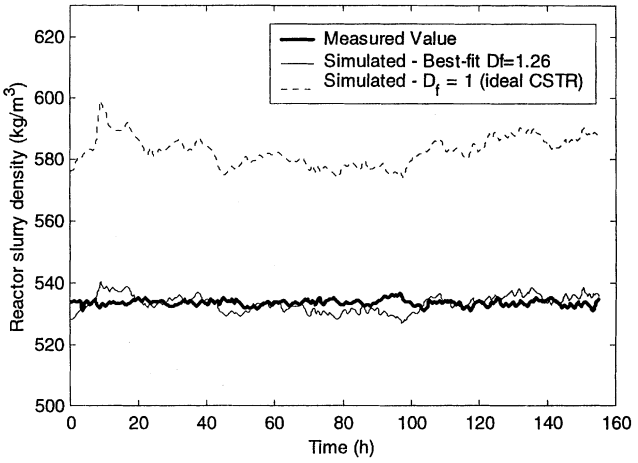

Figure 8. First reactor density for $D_f = 1$ and best-fit value of D_f.

Slurry density is an important controlled variable in the bulk process. It measures the amount of circulating solids in the loop. Bad density control can result in poor reactor productivity or reactor shutdowns due to polymer fouling. Figure 8 shows how the discharge factor (D_f) influences the first reactor slurry density. Notice how an ideal CSTR ($D_f = 1$) is unable to properly model the system, while a nonideal CSTR with $D_f = 1.26$ reproduces the experimental values quite well.

Hydrogen effect on polymer production

Equation 39 shows that the rate of polymerization increases with hydrogen concentration. Plant data show this effect to be both reversible and asymptotic at high hydrogen levels. At low hydrogen concentrations, a small increase in hydrogen content is responsible for a high increase in polymerization rate. At high hydrogen concentrations, this effect is much smaller, or even nonexistent. This type of behavior can be seen in Figure 9.

Effect of process inputs

Figure 10 presents process input changes during a typical industrial campaign of about 2 weeks. Reactor residence time and hydrogen concentrations in both reactors are varied in order to produce polymer grades with different molecular-weight distributions.

Figure 11 shows how the instantaneous production in both reactors is modeled without the inclusion of hydrogen rate-enhancement effects. At low hydrogen concentrations, the simulated production turns out to be higher than the measured one, whereas at high hydrogen concentrations, the opposite behavior is observed.

A kinetic parameter estimation was performed under the hypothesis of ideal CSTR (D_f equal to unity) and includes the hydrogen-effect mechanism. Measured vs. simulated instantaneous reactor production, melt flow index at second reactor output, and slurry densities are shown in Figures 12, 13, and 14, respectively. It can be seen that, although production and MFI show good agreement between experiments and

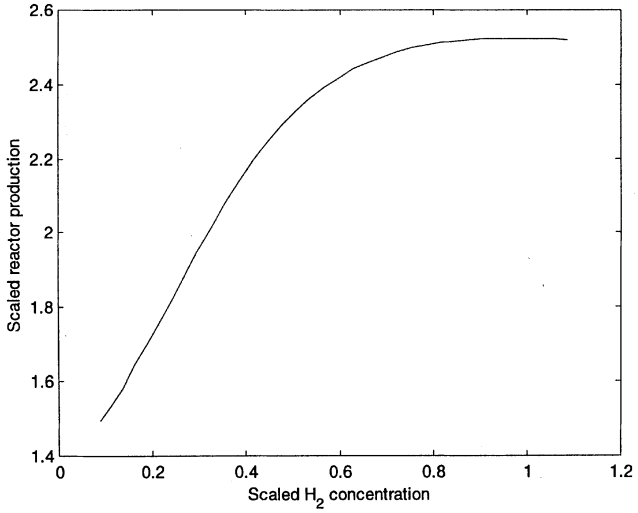

Figure 9. Steady-state production vs. hydrogen concentration.

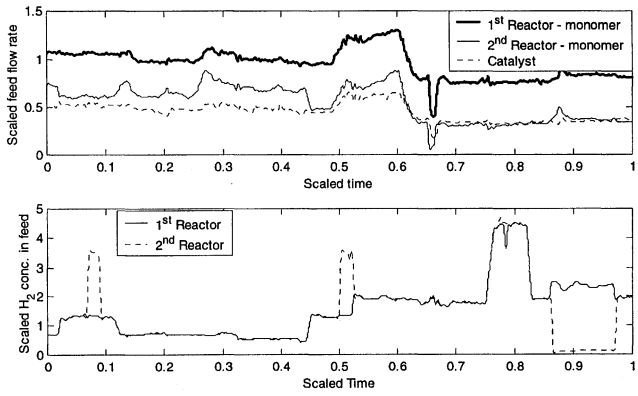

Figure 10. Main process inputs.

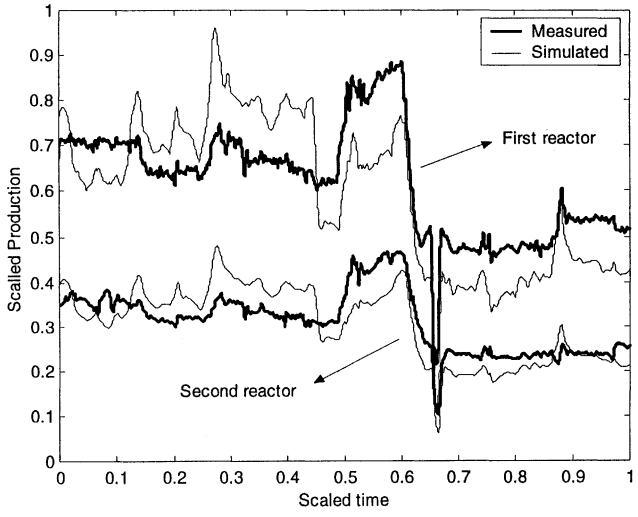

Figure 11. Measured and simulated production with no hydrogen effects.

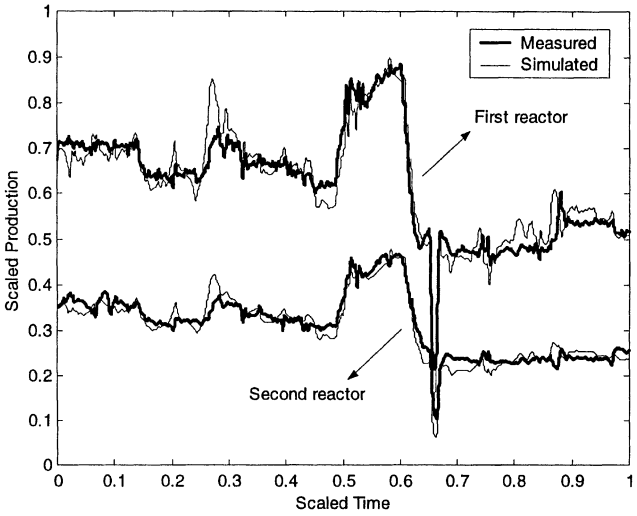

Figure 12. Measured and simulated production for an ideal CSTR.

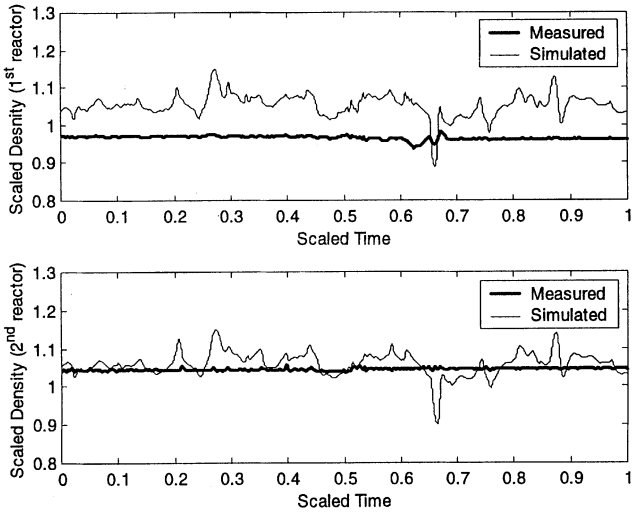

Figure 14. Measured and simulated densities for an ideal CSTR.

simulation, first reactor slurry density still exhibits some bias with respect to measured values.

This bias may be minimized through the estimation, using the same process data, of a different discharge factor for each reactor. Although density bias was removed, it presents oscillations around its actual value, probably because of the input variables noise, as shown in Figure 15. First and second reactor discharge factors are 1.25 and 1.10 respectively, as presented in Table 4 together with the main model parameters and operating conditions. This indicates that polymer weight fractions of both reactors are greater in the output than into reactors, and this effect is more important in the first one. Polymer production and MFI present similar results, as in the case of an ideal CSTR (Figures 16, 17).

Conclusions

A dynamic mathematical model for nonideal loop reactors was presented. The nonideal CSTR model presents some advantages over the traditional CSTR and tubular reactor approaches. On the one hand, it avoids the lengthy simulations involved in tubular-reactor distributed-parameter modeling, while on the other hand, it captures the size selection effects associated with the behavior of industrial equipment. The model is capable of better representing industrial data, especially the reactor slurry-density differences that are observed in practice. A mechanism to take into account the highly nonlinear hydrogen effect in the rate of polymerization was introduced and showed to fit plant data quite well. Hydrogen rate-enhancement effects are very important in industrial polypropylene plants. Polymerization rates can double as a result of increases in typical hydrogen concentration levels. Polymer melt flow index (MFI), a very important product quality-control variable, was successfully modeled as a power function of the mass average molecular weight. Results show that this correlation is valid over a wide range of MFI values.

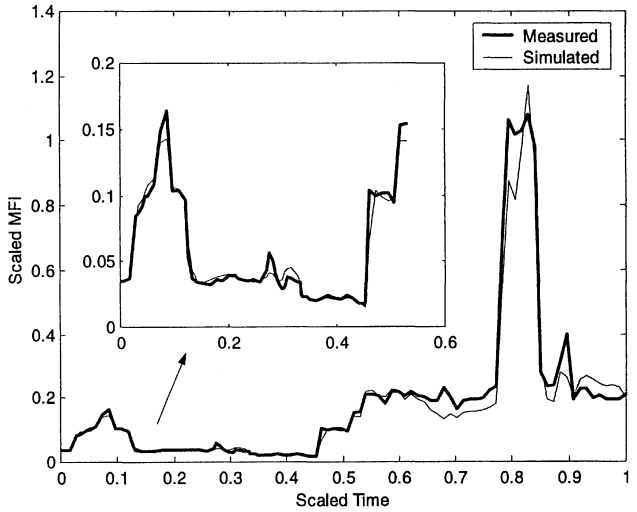

Figure 13. Measured and simulated melt flow index for an ideal CSTR.

Acknowledgments

The authors thank CAPES for financial support and OPP Química S.A. for plant data and permission to publish it.

Notation

A_f = heat exchange area, m^2
B_n^k = bulk polymer concentration, kgmol/m^3
C = total active site concentration, kgmol/m^3
C_d = dead-site concentration, kgmol/m^3
C_j = component j bulk concentration, kgmol/m^3
$C_{j,a}$ = component j concentration at amorphous polymer phase (effective concentration), kgmol/m^3
$C_{j,f}$ = component j concentration at feed stream, kgmol/m^3
$C_{j,l}$ = liquid-phase concentration of component j, kgmol/m^3
$C_{j,R}$ = concentration into the reactor, kgmol/m^3
C^k = type k active specie concentration, kgmol/m^3
C_P = potential site concentration, kgmol/m^3
C_{P_j} = component j specific heat, J/kgK
C_{pm} = mixture specific heat, J/kgK
C_{Pw} = cooling water specific heat, J/kgK
D_f = discharge factor

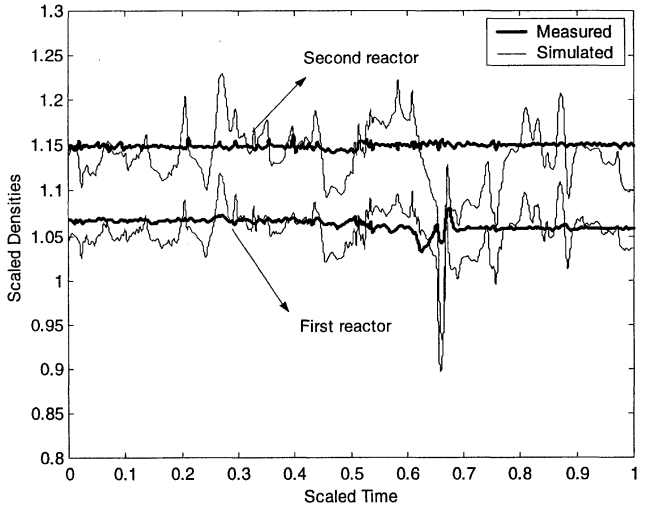

Figure 15. Measured and simulated slurry densities for a nonideal CSTR.

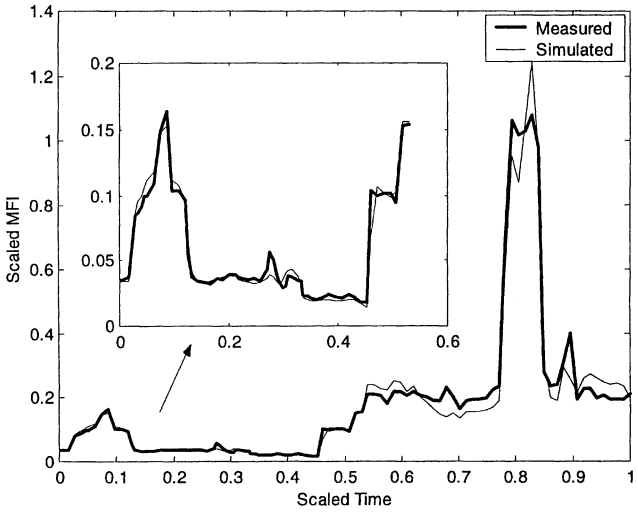

Figure 17. Measured and simulated melt flow index for a nonideal CSTR.

$D_{\boldsymbol{n}}^{k}$ = dead polymer chain concentration with $\boldsymbol{n}$ monomers originated from site k, kgmol/m^3
f_c = polymer crystallinity
ΔH = heat of polymerization, kJ/kgmol
K = two-site equilibrium constant, kgmol^{-1}
$k_{r,i}^{k}$ = kinetic constant for reaction r with end-group i and site k, order dependent
$\dot{m}_{C3,f}$ = monomer feed flow rate, kg/s
$\dot{m}_{CAT,f}$ = catalyst feed flow rate, kg/s
MFI = melt flow index, g/10 min
$\overline{M}_j$ = component j molecular weight, kg/kgmol
$\overline{M}_n$ = number average molecular weight for bulk polymer, kg/kgmol
$\overline{M}w$ = mass average molecular weight, kg/kgmol
$\boldsymbol{n}$ = vector containing the number of each monomer in a polymer chain
NC = number of liquid-phase components
$n_{j,R}$ = moles of component j into reactor, kgmol
$n_{j,a}$ = moles of j sorbed in the amorphous polymer phase, kgmol
$n_{j,l}$ = moles of j in the liquid phase, kgmol

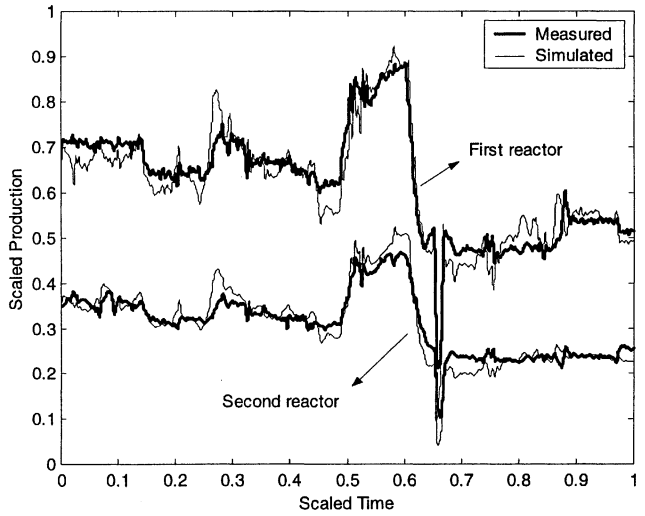

Figure 16. Measured and simulated production for a nonideal CSTR.

Nm = number of monomers
Ns = number of sites
O_r^k = order of reaction r for site k
P_1, P_2 = first and second reactor production, kg/s
$P_{\boldsymbol{n},i}^{k}$ = growing polymer chain with $\boldsymbol{n}$ monomers with end-group i from site k, kgmol/m^3
P_0^k = vacant site k concentration, kgmol/m^3
Q_w = coolant-water volumetric flow rate, m^3/s
Q_f = feed volumetric flow rate, m^3/s
Q_o = reactor-output volumetric flow rate, m^3/s
Q_R = volumetric recirculation flow rate, m^3/s
R_{ec} = recycle ratio
R_j = j component reaction rate, kgmol/(s·m^3)
$R_r^{k,\boldsymbol{n}}$ = r reaction from site k for a growing chain with $\boldsymbol{n}$ monomers, kgmol/(s·m^3)
t = time, s
T = reactor temperature, K
T_w = coolant-water temperature, K
T_{wf} = feed coolant reactor temperature, K
T_f = feed stream temperature, K
U = global heat-exchange coefficient, J/m^{2}Ks
V_R = reactor volume, m^3
$V_{a,m}$ = volume of amorphous polymer phase with monomers absorbed, m^3
V_c = crystalline phase volume, m^3
V_l = liquid-phase volume, m^3
$V_{l,a}$ = volume of liquid phase in amorphous polymer phase, m^3
V_{Pm} = polymer plus absorbed liquid-phase volume, m^3
$V_{P,s}$ = dried polymer volume, m^3
V_w = jacket volume, m^3
$w_{j,f}$ = feed-stream component j weight fraction
$w_{j,l,o}$ = mass fraction of j liquid-phase component in liquid phase at reactor output
$w_{j,l,R}$ = mass fraction of j liquid-phase component in liquid phase into reactor
$w_{j,P,o}$ = mass fraction of j solid-phase component in solid phase at reactor output
$w_{j,P,R}$ = mass fraction of j solid-phase component in solid phase into reactor
$Wl_{j,o}$ = mass concentration of j liquid-phase component at output reactor flow, kg of j/m^3
$Wl_{j,R}$ = mass concentration of j liquid-phase component into reactor, kg of j/m^3
$w_{P,o}$ = polymer weight fraction at reactor output
$w_{P,R}$ = polymer weight fraction into reactor
$Ws_{j,o}$ = mass concentration of j solid-phase component at output reactor flow, kg of j/m^3

$Ws_{j,R}$ = mass concentration of j solid-phase component into reactor, kg of j/m^3
X = poison, poison concentration, kgmol/m^3
Z_P = polydispersity index

Greek letters

γ_j = equilibrium constant for j component between liquid phase and amorphous polymer phase
ζ = ratio between solid-phase components concentration at reactor output flow and into reactor
η = ratio between liquid-phase components concentration at reactor output flow and into reactor
χ = volume fraction of monomer in the amorphous polymer phase
ρ_l = liquid-phase density, kg/m^3
ρ_P = polymer density, kg/m^3
ρ_R = reactor slurry density, kg/m^3
ϕ_P = polymer volumetric fraction

Literature Cited

Bremner, T., and A. Rudin, "Melt Flow Index and Molecular Weight Distributions of Commercial Thermoplastics," *J. Appl. Polym. Sci.*, **41**, 1617 (1990).

Carvalho, A. B., P. E. Gloor, and A. E. Hamielec, "A Kinetic Mathematical Model for Heterogeneous Ziegler-Natta Copolymerization," *Polymer*, **30**, 280 (1989).

Chen, C. M., *Gas Phase Olefin Copolymerization with Ziegler-Natta Catalysts*, PhD Thesis, Univ. of Wisconsin, Madison (1991).

Corradini, P., V. Busico, L. Cavallo, G. Guerra, M. Vacatello, and V. Venditto, "Structural Analogies Between Homogeneous and Heterogeneous Catalyst for the Stereospecific Polymerization of 1-Alquenes," *J. Mol. Catal.*, **74**, 433 (1992).

Ferrero, M. A., and M. G. Chiovetta, "Preliminary Design of a Loop Reactor for Bulk Propylene Polymerization," *Polym. Plast. Technol. Eng.*, **29**(3), 263 (1990).

Froment, G. F., and K. B. Bischoff, *Chemical Reactor Analysis and Design*, Wiley, New York (1979).

Hutchinson, R., *Modeling of Particle Growth in Heterogeneous Catalyzed Olefin Polymerization*, PhD Thesis, Univ. of Wisconsin, Madison (1990).

Galli, P., and Ali, S., "The Spheripol Process: A Versatile Technology for Advanced Polypropylene Property Materials," AIChE Meeting, New York (1987).

Kim, J. Y., and K. Y. Choi, "Modeling of Particle Segregation Phenomena in a Gas Phase Fluidized Bed Olefin Polymerization Reactor," *Chem. Eng. Sci.*, **56**, 4069 (2001).

Lepski, D. M., and A. M. Inkov, "Mathematical Modelling of Polymerization of Propylene in Loop Reactors," *Sb. Tr. Vses. Ob'edin. Neftekhlin*, **13**, 34 (1977).

Liang, W., Y. Jin, Z. Yu, Z. Wang, J. Zhu, and J. Chen, "Flow Characteristics and Mixing Properties in a High Velocity Liquid-Solid Loop Reactor," *Chem. Eng. J.*, **63**, 181 (1996).

Mattos Neto, A. G., and J. C. Pinto, "Steady-State Modeling of Slurry and Bulk Propylene Polymerizations," *Chem. Eng. Sci.*, **56**, 4043 (2001).

Mori, H., M. Endo, K. Tashino, and M. Terano, "Study of Activity Enhancement by Hydrogen in Propylene Polymerization Using Stopped-Flow and Conventional Methods," *J. Mol. Catal. A: Chem.*, **145**, 153 (1999).

Parson, L. W., and T. M. Al-Turki, "On the Mechanism of Action of Hydrogen Added to Propene Polymerizations Using Supported Titanium Chloride Catalysts with a Phthalate Ester/Silane Stereoregulating Donor Pair," *Polym. Commun.*, **30**(3), 72 (1989).

POPS Polyolefins Planning Service, *Global Commercial Analysis*, Report 2, Chem Systems Inc., White Plains, NY (2000).

Reginato, A. S., *Modelagem e Simulação dos Reatores de Polimerização em Fase Líquida do Processo Spheripol*, Masters Thesis, UFRGS/RS, Brazil (2001).

Rishina, L. A., E. I. Visen, L. N. Sosnovskaja, and F. S. Dyachkovsky, "Study of the Effect of Hydrogen in Propylene Polymerization with the $MgCl_2$-Supported Ziegler-Natta Catalyst—Part 1. Kinetics of Polymerization," *Eur. Polym. J.*, **30**, 1309 (1994).

Samson, J. B., P. J. Bosmam, G. Weickert, and K. R. Westerterp, "Liquid-Phase Polymerization of Propylene with a Highly Active Ziegler-Natta Catalyst. Influence of Hydrogen, Cocatalyst and Electron Donor on the Reaction Kinetics," *J. Polym. Sci.*, **37**, 219 (1999).

Secchi, A. R., and A. Bolsoni, "Otimização das Condições Operacionais de um Reator Tubular de PEBD," *COBEQ'98*, Porto Alegre, Brasil (1998).

Shampine, L. F., and M. W. Reichelt, *The MATLAB ODE Suite*, Southern Methodist Univ., Dallas, and The Mathworks Inc., Natick, MA (1997).

Soares, J. P., and A. E. Hamielec, "Effect of Hydrogen and of Catalyst Prepolymerization with Propylene on the Polymerization Kinetics of Ethylene with a Non-supported Heterogeneous Ziegler-Natta Catalyst," *Polymer*, **37**, 4599 (1996a).

Soares, J. B. P., and A. E. Hamielec, "Copolymerization of Olefins in a Series of Continuous Stirred-Tank Slurry-Reactors Using Heterogeneous Ziegler-Natta Catalyst. 1. General Dynamic Mathematical Model," *Polym. React. Eng.*, **4**(2&3), 153 (1996b).

Uvarov, B. A., and V. I. Tsevetkova, "Development of a Mathematical Model for Controlling the Yield of Propylene Polymerization in Loop Reactors," *Polim. Protsessy Appar.*, 165 (1974).

Zacca, J. J., *Modelling of the Liquid Phase Olefin Polymerization in Loop Reactors*, Master Thesis, Univ. of Wisconsin, Madison (1991).

Zacca, J. J., and W. H. Ray, "Modelling of the Liquid Phase Polymerization of Olefins in Loop Reactors," *Chem. Eng. Sci.*, **48**, 3743 (1993).

Zacca, J. J., *Distributed Parameter Modelling of the Polymerization of Olefins in Chemical Reactors*, PhD Thesis, Univ. of Wisconsin, Madison (1995).

Zacca, J. J., and J. A. Debling, "Particle Population Overheating Phenomena in Olefin Polymerization Reactors," *Chem. Eng. Sci.*, **56**, 4029 (2001).

Appendix A

In order to derive Eqs. 22 and 23, a molar balance for component j is performed

$$n_{j,R} = n_{j,l} + n_{j,a} \tag{A1}$$

where

$$n_{j,R} = C_{j,R} V_R \tag{A2}$$

$$n_{j,a} = C_{j,a} V_{a,m} \tag{A3}$$

From Eq. A1 to Eq. A3 and using Eq. 20, $C_{j,a} = \gamma_j C_{j,l}$

$$\frac{C_{j,a}}{C_j} = \frac{V_R}{V_{a,m}} \frac{\gamma_j \dfrac{V_{a,m}}{V_l}}{1 + \gamma_j \dfrac{V_{a,m}}{V_l}} \tag{A4}$$

Equation A4 represents the ratio between the number of moles of j in the amorphous polymer phase and the total number of moles of j.

The total reactor volume V_R is the sum of the liquid-phase volume and the polymer volume. The polymer-phase volume is given by the sum of the dry polymer volume and its corresponding sorbed liquid phase ($V_{l,a} = \chi V_{a,m}$). Therefore

$$V_R = V_l + V_{p,s} + \chi V_{a,m} \tag{A5}$$

Since $V_{p,s}(1-f_c)=V_{a,m}(1-\chi)$, the total reactor volume can be expressed by the following equation

$$V_R = V_l + \frac{(1-\chi)V_{a,m}}{1-f_c} + \chi V_{a,m} \tag{A6}$$

From Eqs. A4 and A6, it is possible to write

$$\frac{C_{j,a}}{C_j} = \left(\frac{V_l}{V_{a,m}} + \frac{1-\chi}{1-f_c} + \chi\right)\frac{\gamma_j \dfrac{V_{a,m}}{V_l}}{1+\gamma_j \dfrac{V_{a,m}}{V_l}} \tag{A7}$$

where the ratio $V_l/V_{a,m}$ can be obtained from Eq. A5

$$\frac{V_R}{V_{a,m}}\frac{V_{p,s}}{V_{p,s}} = \frac{V_l}{V_{a,m}} + \frac{V_{p,s}}{V_{a,m}} + \chi\frac{V_{a,m}}{V_{a,m}} \tag{A8}$$

By defining the volumetric polymer fraction as $\phi_P = (V_{P,s}/V_R)$, Eq. A8 yields

$$\frac{V_l}{V_{a,m}} = \frac{1-\chi}{1-f_c}\left(\frac{1}{\phi_P} - 1\right) - \chi \tag{A9}$$

Appendix B

The mass concentrations of component j inside the reactor and at the reactor outflow are given by Eqs. B1 and B2

$$Wl_{j,R} = \rho_R(1-w_{P,R})w_{j,l,R} \tag{B1}$$

$$Wl_{j,o} = \rho_o(1-w_{P,o})w_{j,l,o} = \rho_o\left(1-D_f w_{P,R}\right)w_{j,l,o} \tag{B2}$$

where $w_{j,l,R}$ and $w_{j,l,o}$ represent the mass fraction of component j in the reactor liquid phase and at the reactor outflow.

Considering that the liquid phase composition in the reactor equals the liquid-phase composition at the reactor outlet ($w_{j,l,R}=w_{j,l,o}$)

$$\eta = \frac{Wl_{j,o}}{Wl_{j,R}} = \frac{C_{j,o}}{C_{j,R}} = \frac{\rho_o}{\rho_R}\frac{1-D_f w_{P,R}}{1-w_{P,R}} \tag{B3}$$

For the solid phase, one can write

$$Ws_{j,R} = \rho_R w_{P,R} w_{j,P,R} \tag{B4}$$

$$Ws_{j,o} = \rho_o w_{P,o} w_{j,P,o} = \rho_o D_f w_{P,R} w_{j,P,o} \tag{B5}$$

where $w_{j,P,R}$ and $w_{j,P,o}$ represent the solid-phase mass fraction of component j.

Supposing that the solid-phase composition in the reactor equals the solid-phase composition at the reactor outlet ($w_{j,P,R}=w_{j,P,o}$); it is then possible to write

$$\zeta = \frac{Ws_{j,o}}{Ws_{j,R}} = \frac{C_{j,o}}{C_{j,R}} = \frac{\rho_o}{\rho_R}D_f \tag{B6}$$

Appendix C

In the case of homopolymerization with two types of catalyst sites, the rate of polymerization at each site is given by

$$R_P^1 = k_P^1 C^1 C_{M,a} \tag{C1}$$

$$R_P^2 = k_P^2 C^2 C_{M,a} \tag{C2}$$

Hydrogen is supposed to participate in the following two-site equilibrium

$$C^1 + H_2 \xrightarrow{k_a} C^2 \tag{C3}$$

$$C^2 \xrightarrow{k_{-a}} C^1 + H_2 \tag{C4}$$

A balance for site type 1 under the quasi-steady-state hypothesis yields

$$\frac{dC^1}{dt} = -k_a C^1 C_{H,a} + k_{-a} C^2 = 0 \tag{C5}$$

By defining

$$K = \frac{k_a}{k_{-a}} = \frac{C^2}{C^1 \cdot C_{H,a}}$$

as the equilibrium constant and $C = C^1 + C^2$ as the total sites concentration, it follows that

$$C^1 = \frac{C}{1+K\cdot C_{H,a}} \tag{C6}$$

The total rate of polymerization is the sum of the rate of polymerization at each site type

$$R_P = R_P^1 + R_P^2 = k_P^1 C^1 C_{M,a} + k_P^2 C^2 C_{M,a} = C^1 C_{M,a}\left(k_P^1 + k_P^2 K C_{H,a}\right) \tag{C7}$$

From Eqs. C6 and C7

$$R_P = k_P^1 \frac{1+K\dfrac{k_P^2}{k_P^1}C_{H,a}}{1+K\cdot C_{H,a}} C\cdot C_{M,a} = k_{P,r} C\cdot C_{M,a} \tag{C8}$$

Manuscript received Apr. 10, 2002, and revision received Mar. 6, 2003.